

Towards viscoplastic constitutive models for Cosserat rods

Vanessa Dörlich^{##}, Joachim Linn[#], Tobias Scheffer^{*}, Stefan Diebels^{*}

[#] Department Mathematical Methods in Dynamics and Durability
Fraunhofer Institute for Industrial Mathematics ITWM
Fraunhofer Platz 1, D-67663 Kaiserslautern, Germany
[vanessa.doerlich, joachim.linn]@itwm.fraunhofer.de

^{*} Lehrstuhl für Technische Mechanik
Universität des Saarlandes
Campus A4 2, D-66123 Saarbrücken, Germany
[s.diebels, t.scheffer]@mx.uni-saarland.de

ABSTRACT

Flexible, slender structures like cables, hoses or wires can be described by the geometrically exact Cosserat rod theory. Due to their complex multilayer structure, consisting of various materials, viscoplastic behavior has to be expected for cables under load. Classical experiments like uniaxial tension, torsion or three-point bending already show that the behavior of e.g. electric cables is viscoplastic. A suitable constitutive law for the observed load case is crucial for a realistic simulation of the deformation of a component. Consequently, this contribution aims at a viscoplastic constitutive law formulated in the terms of sectional quantities of Cosserat rods. Since the loading of cables in applications is in most cases not represented by these mostly uniaxial classical experiments, but rather multiaxial, new experiments for cables have to be designed. They have to illustrate viscoplastic effects, enable access to (viscoplastic) material parameters and account for coupling effects between different deformation modes. This work focuses on the design of such experiments.

Keywords: Cosserat rods, viscoplasticity, multiaxial experiments, flexible structures, cables.

1 INTRODUCTION

Cables and hoses are slender flexible objects and can be described physically correctly by the geometrically exact theory of Cosserat rods [1]. The principal constituents of the rod model are geometrically exact kinematics relating configuration variables and objective strain measures, balance equations that govern the dynamic equilibrium of the sectional quantities, and constitutive equations, which yield the sectional forces and moments in terms of the deformation. Finding an appropriate constitutive model is especially necessary to enable a realistic simulation of the deformation behavior of a structure. A viscoelastic model formulated in the sectional force and moment quantities and objective deformation measures of the Cosserat rod model was already presented in [2] and [3]. In this contribution, we focus on viscoplastic effects and present first steps towards an application oriented modeling approach on the level of sectional quantities similar to Simo et al. [4].

Cables and hoses are components with a complex multilayer structure, which consists for example of parallel or twisted wires, insulating layers, woven fabrics and sheaths. Their behavior under load can thus be investigated on different scales, for example on the microscale if single wires are considered or on the macroscale by observing the deformation of whole cables. Due to various effects like friction between the constituents, pull-out of wires or delamination, a treatment on the microscale and subsequent coupling of the effects is computationally too complex. Furthermore, these effects cannot be measured in experiments on the microscale. Therefore, the deformation of cables and hoses will be investigated and modeled phenomenologically on the level of sectional quantities.

Since cables include a variety of materials like ductile metals, (hyper-)elastic polymers or brittle glass fibers, it is not sufficient to use linear-elastic constitutive models if a realistic simulation is the aim. Inelastic behavior like viscosity, plasticity and friction cannot be neglected. This can already be seen when classical experiments like uniaxial tension, torsion or three-point bending tests are executed cyclically, which will be shown in section 2.5. These classical tests provide information about the tensile, torsional and bending stiffness of the specimens. However, they do not represent realistic loading situations of cables in applications, which are mostly multiaxial and combine several of the classical load cases. Therefore, multiaxial experiments providing information about the coupling of the single stiffnesses have to be executed. Section 2.5.2 deals with the design of suitable multiaxial experiments for the characterization of cables and hoses. In a first approach, we test straight clamped cables and hoses in large deformation experiments combining bending, torsion and tension after van der Heijden et al. [5, 6]. Since these experiments will prove to be not useful for characterizing cables and hoses, new simplified multiaxial experiments for clamped cables are designed.

2 BASIC CONSIDERATIONS ON MODELING AND EXPERIMENTS

2.1 Kinematics of Cosserat rods

The kinematics of a Cosserat rod are described by its configuration variables, see figure 1. The centerline curve $\mathbf{r}(s)$ and the moving frame $\hat{\mathbf{R}}(s)$ are both a function of the arc length s in the reference configuration [7]

$$s \mapsto \mathbf{r}(s) \in \mathbb{R}^3, \quad (1)$$

$$s \mapsto \hat{\mathbf{R}}(s) \in SO(3). \quad (2)$$

The orthonormal set of vectors $\mathbf{a}^{(\alpha)}$ defines the cross section where $\mathbf{a}^{(1)}$ and $\mathbf{a}^{(2)}$ span the cross section and $\mathbf{a}^{(3)}$ is the normal vector. The material strain measures related to the configuration

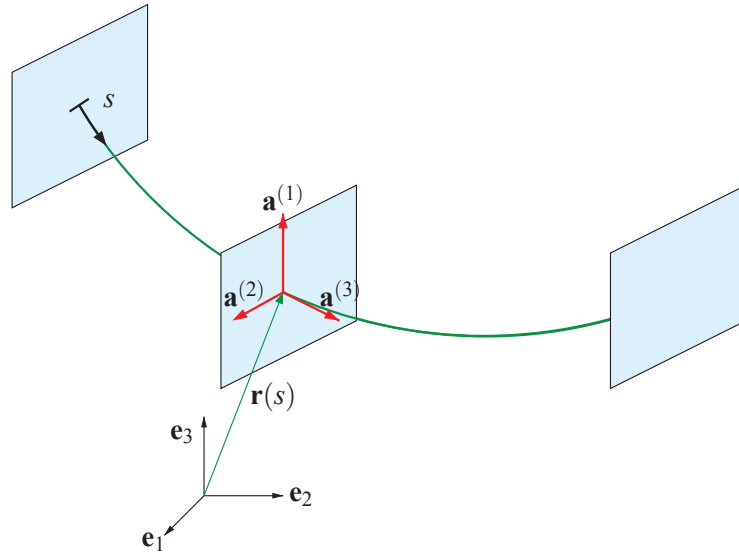


Figure 1: The kinematics of Cosserat rods.

variables are

$$\begin{aligned} K^{(\alpha)} &:= \langle \mathbf{a}^{(\alpha)}, \mathbf{a}^{(3)} \times \partial_s \mathbf{a}^{(3)} \rangle; & \Gamma^{(\alpha)} &:= \langle \mathbf{a}^{(\alpha)}, \partial_s \mathbf{r} \rangle; & \alpha &= 1, 2 \\ K^{(3)} &:= \mathbf{a}^{(2)} \cdot \partial_s \mathbf{a}^{(1)}; & \Gamma^{(3)} &:= \langle \mathbf{a}^{(3)}, \partial_s \mathbf{r} \rangle - 1. \end{aligned} \quad (3)$$

$K^{(\alpha)}$ measures the bending curvatures for $\alpha = 1, 2$ and $K^{(3)}$ the torsional twist. The transverse shear strain components are given by $\Gamma^{(\alpha)}$ for $\alpha = 1, 2$ and the longitudinal strain is given by $\Gamma^{(3)}$.

An extensible Kirchhoff rod satisfies the additional constraint

$$\mathbf{t} = \frac{\partial_s \mathbf{r}}{\|\partial_s \mathbf{r}\|} \stackrel{!}{=} \mathbf{a}^{(3)} \quad (4)$$

for the tangent vector \mathbf{t} of the centerline, which inhibits transverse shearing by keeping the cross sections of the rod normal to the tangent vector [8]. Consequently, the components of $\mathbf{\Gamma}$ are

$$\Gamma^{(\alpha)} \equiv 0; \quad \alpha = 1, 2 \quad (5)$$

$$\Gamma^{(3)} = \|\partial_s \mathbf{r}\| - 1. \quad (6)$$

2.2 Static equilibrium equations

The system of static equilibrium equations for Cosserat rods

$$\begin{aligned} \partial_s \mathbf{f} + \mathbf{f}_{ext} &= \mathbf{0} \\ \partial_s \mathbf{m} + \partial_s \mathbf{r} \times \mathbf{f} + \mathbf{m}_{ext} &= \mathbf{0} \end{aligned} \quad (7)$$

is valid independent of the constitutive equations. It has to be satisfied by the spatial sectional forces \mathbf{f} and moments \mathbf{m} , which can be resolved with respect to the moving frame according to

$$\mathbf{f} = \hat{\mathbf{R}}(s) \cdot \mathbf{F}; \quad \mathbf{m} = \hat{\mathbf{R}}(s) \cdot \mathbf{M}. \quad (8)$$

2.3 Constitutive laws

The constitutive equations relate the material sectional forces \mathbf{F} and moments \mathbf{M} with the strain measures given in equations (3). A linear-elastic constitutive law formulated in the material sectional quantities is for example

$$\mathbf{F} = \mathbb{C}_F \cdot \mathbf{\Gamma}^{el}; \quad \mathbf{M} = \mathbb{C}_M \cdot \mathbf{K}^{el} \quad (9)$$

with the effective stiffness matrices \mathbb{C}_F and \mathbb{C}_M .

2.4 Formulation of plastic constitutive laws

The simplest case of a rate-independent elasto-plastic constitutive equation can be derived from figure 2 according to [9]. It consists of an elastic spring with Young's modulus E and a Coulomb

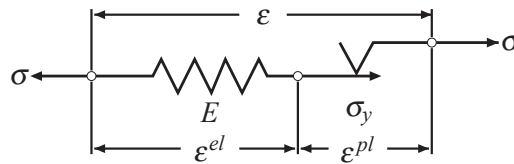


Figure 2: One-dimensional friction device illustrating rate-independent elasto-plasticity, after [9].

friction element with yield stress σ_y . Due to the serial connection, the total strain ε can be split into an elastic and a plastic part

$$\varepsilon = \varepsilon^{el} + \varepsilon^{pl}. \quad (10)$$

The elastic stress on the spring is

$$\sigma = E \varepsilon^{el} \quad (11)$$

and can be formulated with equation (10) as

$$\sigma = E (\varepsilon - \varepsilon^{pl}). \quad (12)$$

The plastic strain ε^{pl} is an additional kinematic variable following the evolution equation

$$\dot{\varepsilon}^{pl} = \frac{\partial}{\partial t} \varepsilon^{pl} = \gamma \frac{\partial f}{\partial \sigma} \quad (13)$$

assuming that ε^{pl} is a function of time t . The evolution equation is called an associative flow rule, if the potential relationship in equation (13) holds for the yield function f , γ is a plastic multiplier. The yield function serves as a criterion for determining the occurrence of yield at a certain load. Algorithmic approaches to solve elasto- or viscoplastic problems can be found exemplarily in [9, 10].

Similar to equation (12), rate-independent elasto-plastic constitutive laws can be formulated in terms of the sectional forces and moments as

$$\mathbf{F} = \mathbb{C}_F \cdot (\boldsymbol{\Gamma} - \boldsymbol{\Gamma}^{pl}); \quad \mathbf{M} = \mathbb{C}_M \cdot (\mathbf{K} - \mathbf{K}^{pl}). \quad (14)$$

The long-term goal of this work is to extend this formulation to rate-dependent viscoplastic constitutive laws for Cosserats rods in terms of sectional quantities.

Remark: The primary interest lies in plastic bending and torsion of cables, since these cases occur more often in applications. Longitudinal extensional and transversal shear strains are assumed as approximately elastic, such that plastic effects herein can be neglected for practical reasons.

2.5 Experimental characterization of cables and hoses

Executing suitable experiments is an important part of modeling the deformation behavior of structural elements. Such experiments have to provide access to the model parameters and have to serve as an appropriate database for simulating a certain load case. The work of several authors has already shown for example that in order to perform multiaxial simulations, it is not sufficient to determine the model parameters in uniaxial experiments [11, 12, 13, 14]. In the first part of this section, classical experiments for the characterization of beam-like structures will be described, which enable access to linear-elastic stiffnesses. They already illustrate the necessity of including inelastic effects in the modeling of cables under load, when they are performed cyclically. However, these experiments are not sufficient to provide information about the coupling of different load cases and do not represent realistic loading of cables in application. Suitable multiaxial experiments combining different load cases have to be designed and executed in order to get information about the coupling of tension, torsion and bending. The second part of this section deals with this issue.

2.5.1 Classical experiments

Classical experiments for the characterization of beam-like structures available in the literature are for example uniaxial tension, torsion and three-point bending tests [15]. Figure 3 shows the schematic setups of the executed experiments. The experimental results can be analyzed under the assumption of linear-elastic behavior from the plot of the measured quantities y and x , see figure 4. The tensile stiffness $(EA)_{uni}$, the torsional stiffness $(GJ)_T$ or the bending stiffness $(EI)_B$ can be calculated respectively by a linear relation according to

$$y = kx \quad (15)$$

from the linear slope k as shown in table 1. The stiffnesses $(EA)_{uni}$, $(GJ)_T$ and $(EI)_B$ are rather component specific parameters than material parameters. They include information about the geometry of the cable in form of the cross section area A , the area moment of inertia I and the polar moment of inertia J in addition to the material parameters E , the Young's modulus, and G , the shear modulus.

These classical experiments already enable access to the stiffnesses for linear-elastic constitutive models. By executing several consecutive cycles, they even provide information about the inelastic behavior of cables.

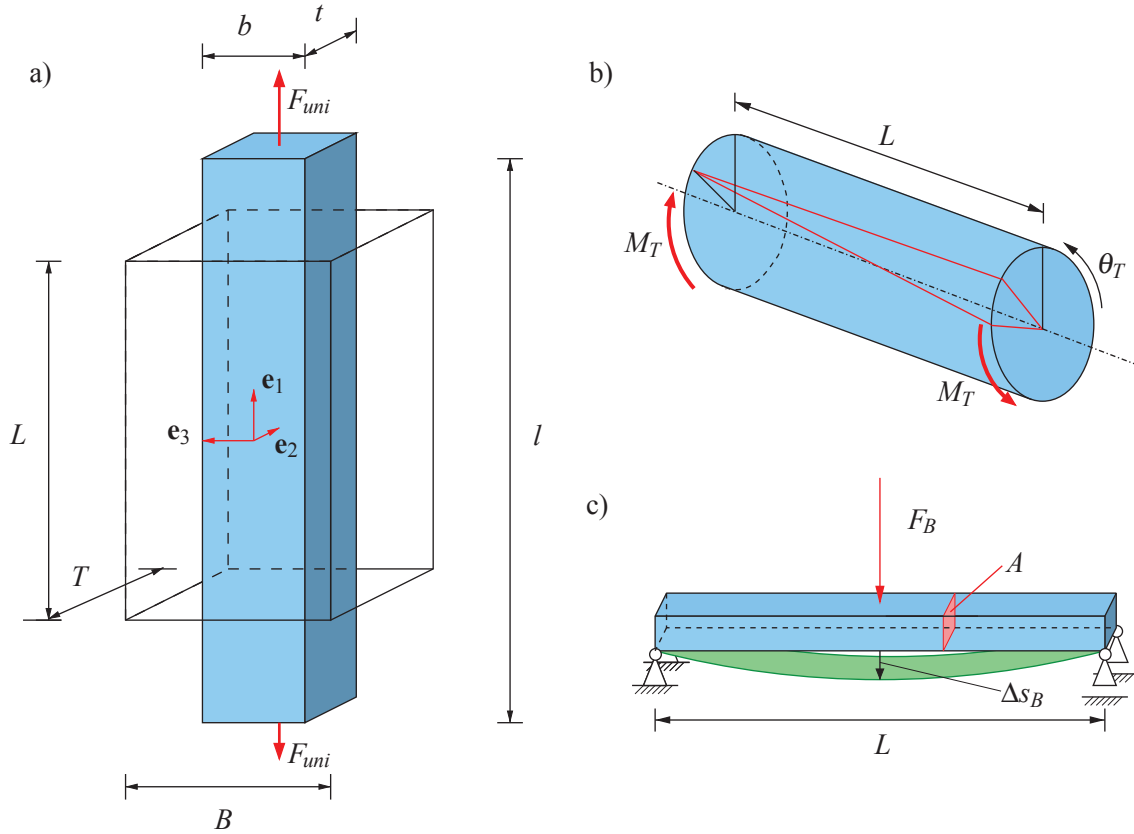


Figure 3: Schematic setups of a) uniaxial tension, b) torsion and c) three-point bending tests.

2.5.2 Multiaxial experiments

In order to get information about the coupling of different load cases, it is necessary to test cables in multiaxial experiments.

Van der Heijden et al. [5, 6] describe the writhing of cylindric metallic wires as multiaxial experiments for clamped rods. The experimental procedure is shown in figure 5. The ends of the specimen are clamped in one axis, the specimen is twisted about this axis and afterwards one clamp is moved towards the other clamp. These experiments are executed for several torsion angles. After Euler's Theory of the elastica [16, 17], primary buckling of an untwisted specimen of length L and bending stiffness $(EI)_B$ into a planar configuration occurs at a critical load T according to

$$t = \frac{TL^2}{4\pi^2 (EI)_B} = -1. \quad (16)$$

Pretwisted specimens will buckle directly into a spatial configuration where bending, torsion and - in certain cases - tension couple at another critical load. The ratio of bending to torsional stiffness determines the transition from planar to spatial configurations and vice versa. The final shape of the specimen at maximum displacement D for $D/L = 1$ is a ring for any torsion angle. Stable as well as unstable configurations exist, since different buckling modes are possible.

The spatial configurations as well as the axial forces and moments are measured during the experiment. Van der Heijden et al. compare their experimental results for nitinol wires to semi-analytical computations using an inextensible Kirchhoff rod model (i.e. a constrained variant of the Cosserat rod with inhibited longitudinal extension and transverse shearing). They observe a characteristic shape of the experimental and simulated curves resulting from a normalization of the measured forces on the critical buckling load and the displacement D on the original length, see figure 6. Besides, curves for different original lengths coincide for the same torsion angle.

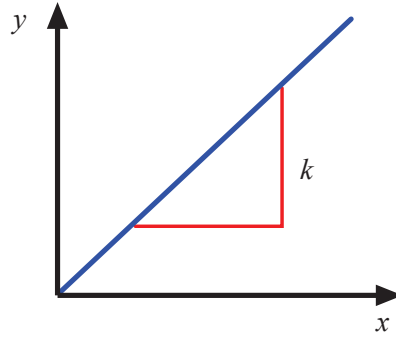


Figure 4: Analysis of experimental results under assumption of linear-elasticity.

Table 1: Measured quantities y , x and value of slope k for classical tests.

| | y | x | k |
|---------|----------------------------------|--------------------------|------------------------|
| tension | uniaxial tensile force F_{uni} | displacement D | $\frac{(EA)_{uni}}{L}$ |
| torsion | torsional moment M_T | torsion angle θ_T | $\frac{(GJ)_T}{L}$ |
| bending | bending force F_B | deflection Δs_B | $\frac{48(EI)_B}{L^3}$ |

In the next step, the multi-axial procedure is simplified by avoiding the possibility of unstable configurations. This is achieved by combining successive steps of torsion and uniaxial tension instead of compression. The torsion and tension steps can be arranged arbitrarily, which reveals different coupling effects.

In this work, two types of experiments are described. The first one is used to investigate the influence of pretorsion on the behavior of the cable under cyclic uniaxial tension. The second one examines the effect of a prestretch on the behavior of the specimen under cyclic torsion.

3 CHARACTERIZATION OF A COAXIAL CABLE

3.1 Experiments

A coaxial cable is characterized using the described classical and multi-axial experiments. The cross section of the cable has a diameter of 2.8 mm and is shown in figure 7.

The cyclic loading in the classical experiments is applied displacement-controlled and 5 cycles are performed in each experiment. The maximum loading is 100 N for the uniaxial tension test, 360° for the torsion test and 6 mm for the three-point bending test. The results of the cyclic classical experiments on a coaxial cable are shown in figure 8. The stiffnesses calculated from the loading paths of the experiments are summarized in table 2, where the values for the first cycle are calculated separately from cycles 2 – 5. This illustrates that especially the torsional and bending stiffnesses change after the first cycle. All three experiments have in common, that the behavior is clearly non-linear and that hysteresis loops appear. The cyclic experiments also give proof of remaining plastic deformation. In the uniaxial tension test, a plastic stretch occurs, which results in a compressive force in order to reach the original length of the specimen. Similarly, a negative torsional moment is necessary during unloading in the torsion test because of a permanent twist. During three-point bending, the punch loses contact to the specimen while unloading at approximately 3 mm due to remaining curvature, see figure 8 d). In case of the uniaxial tension test, a sharp kink at approximately 54 N is visible in the first loading path, which can be interpreted



Figure 5: Experimental procedure of multiaxial experiment: A straight specimen is clamped (left), the upper clamp is rotated by 4π (middle) and afterwards moved down by 60 mm (right).

as a yield point for the tensile load case. To determine if this kink is the tensile yield point for this cable, cyclic uniaxial tension with a maximum axial force of 40 N has been executed. The result is shown in figure 8 in comparison to the loading up to 100 N. The expectation is being confirmed because in this case, no yield and nearly no hysteresis appears. Therefore, the yield point was not reached in this experiment.

Table 2: Stiffnesses measured in the classical experiments.

| | $(EA)_{uni}$ [N] | $(GJ)_T$ [N·m ²] | $(EI)_B$ [N·m ²] |
|-------------------------|--------------------|------------------------------|------------------------------|
| 1 st cycle | $2.020 \cdot 10^4$ | $8.235 \cdot 10^{-4}$ | $9.813 \cdot 10^{-4}$ |
| average of cycles 2 – 5 | $2.081 \cdot 10^4$ | $1.078 \cdot 10^{-3}$ | $1.898 \cdot 10^{-4}$ |

The experimental setup by van der Heijden et al. described in section 2.5.2 is used to test the coaxial cable in a realistic multiaxial loading. Pretorsion angles of 0 , π , 2π , 3π and 4π are applied before the upper clamp is moved by 60 mm. Specimens of two different lengths (100 mm and 180 mm) are used. The results are shown in figure 9. The left plot shows the results for a specimen of an initial length of 180 mm for different torsion angles. The shape of the curves differs already qualitatively from the theoretical results shown in figure 6. The right hand figure compares the results for both initial lengths for no pretorsion and 4π pretorsion. In both cases, the measured curves do not coincide after the normalization on length and critical buckling load. These results show that this type of experiment is too complex and its interpretation too complicated to be useful for determining the coupling between the different stiffnesses. Consequently, new simplified multiaxial experiments have to be designed which provide access to the desired information. The experimental procedures of the simplified multiaxial experiments are illustrated in figure 10. To determine the influences of pretorsion and prestretch, different pretorsion angles θ_T from 0° to 360° or different prestretches up to 100 N are applied.

The influence of pretorsion on the behavior of the coaxial cable under tension is shown in figure 11. The uniaxial tensile force F_{uni} is plotted versus the displacement D for different pretorsion angles. The tensile stiffness decreases with increasing pretorsion angles. This effect can be interpreted as a result of delamination and hence softening of the cable during the torsion. This result has to be

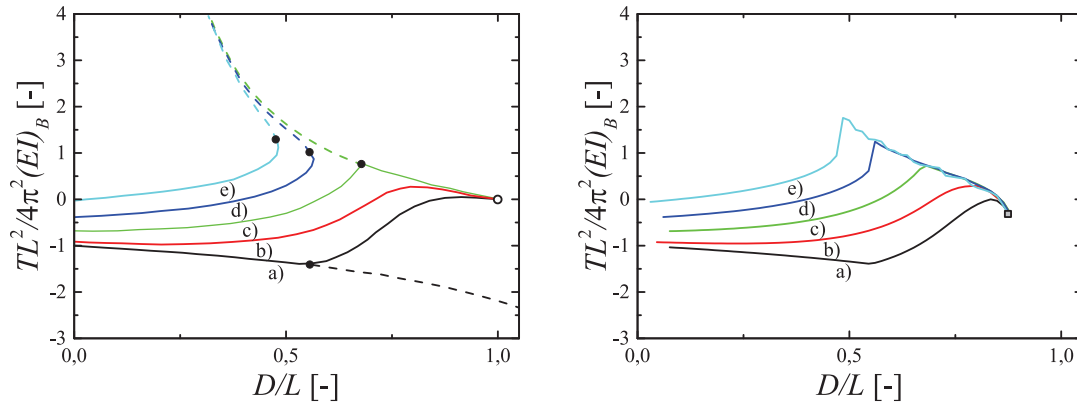


Figure 6: Theoretical results of multi-axial experiments for different torsion angles of a) 0, b) π , c) 2π , d) 3π , e) 4π , after [5] (left) and own results of simulation based on a discrete Cosserat rod model (right). Dashed lines symbolize instable branches, dots mark transition from stable to unstable branches and the circle marks the ring configuration.

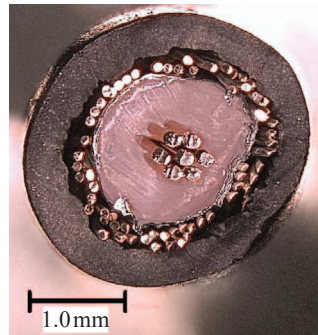


Figure 7: Cross section of investigated coaxial cable.

handled carefully. In a zoomed in plot of the loading path of the first cycle for 0° and 360° it is visible that uniaxial tension force is already applied during the torsion step, see figure 11. Due to the twist, the specimen is elongated effectively, which results in an axial force. Consequently, the softening effect may be a result of the torsion induced pretension and is not a result of pure pretorsion. Therefore, the experimental procedure is slightly adapted in order to avoid this effect. A pure pretorsion load is achieved by activating force control during the pretorsion, which keeps the axial force at zero by adjusting the distance between the clamps. Besides, force control is already activated during the clamping of the specimen in order to avoid tensile forces on the specimen before testing. The adapted experimental procedure and resulting curves of uniaxial tension force are shown in figure 12. The same tendency is visible. An increasing pretorsion causes a decreasing tensile stiffness. Now, this result is only due to the combination of pure pretorsion and uniaxial tension. The pretorsion influences another inelastic feature, the hysteresis loops grow larger with increasing pretorsion, which is equivalent to an increasing dissipation. The aforementioned kink in the first loading path of the uniaxial tension is as well visible for the pretwisted specimens.

The influence of prestretch on the torsion behavior of the coaxial cable is shown in figure 13. The torsional moment M_T is plotted versus the torsion angle θ_T for different prestretches up to a certain maximum force. No influence of different prestretches on the size of the hysteresis loops or the slope is visible. Consequently, the torsion behavior and plasticity of this cable are not a function of prestretch.

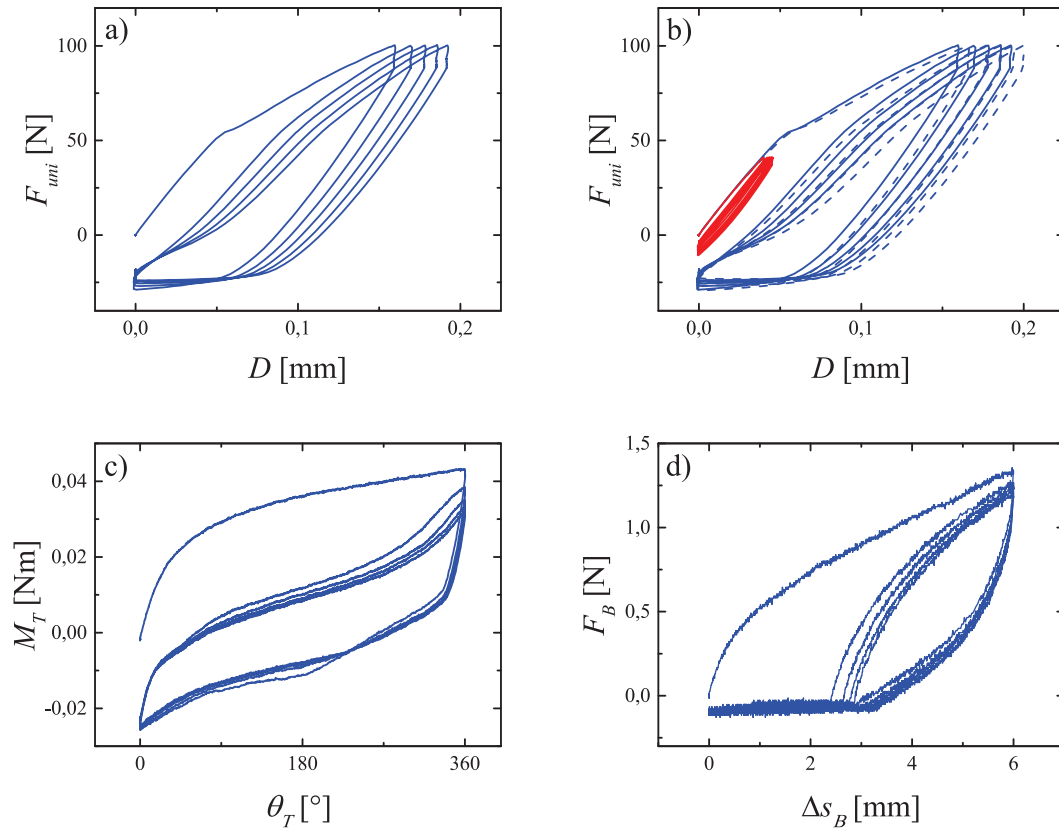


Figure 8: Results of cyclic classical experiments on a coaxial cable: a) uniaxial tension test, b) uniaxial tension including test for yield point, c) torsion test, d) three-point bending.

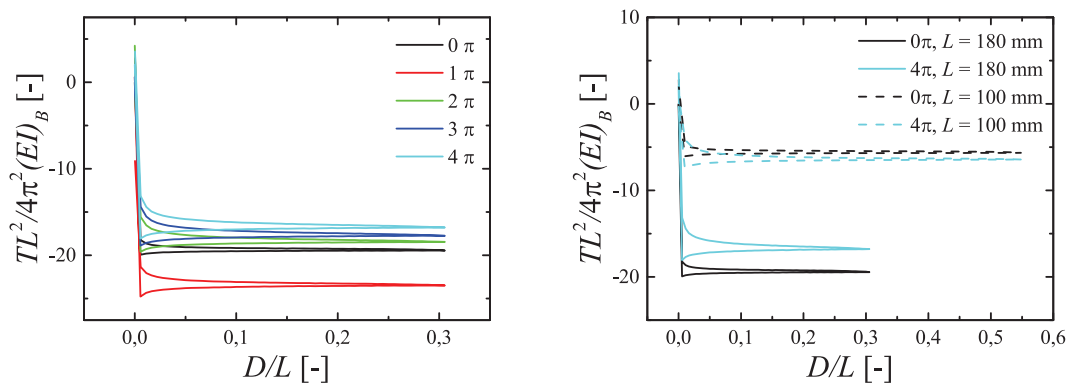


Figure 9: Results of multiaxial experiment on coaxial cable. Left: Comparison of different torsion angles for specimen of length 180 mm. Right: Comparison of results for specimens of both lengths for torsion angles of 0 and 4π .

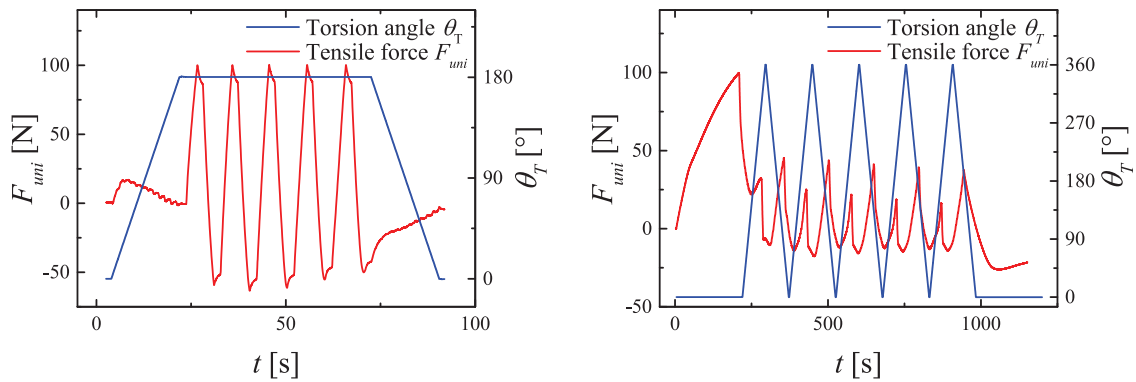


Figure 10: Experimental procedure of multiaxial experiments combining tension and torsion. Left: A pretorsion of 180° is applied before cyclic uniaxial tension. Right: The specimen is prestretched until $F_{uni} = 100\text{N}$ before cyclic torsion is applied.

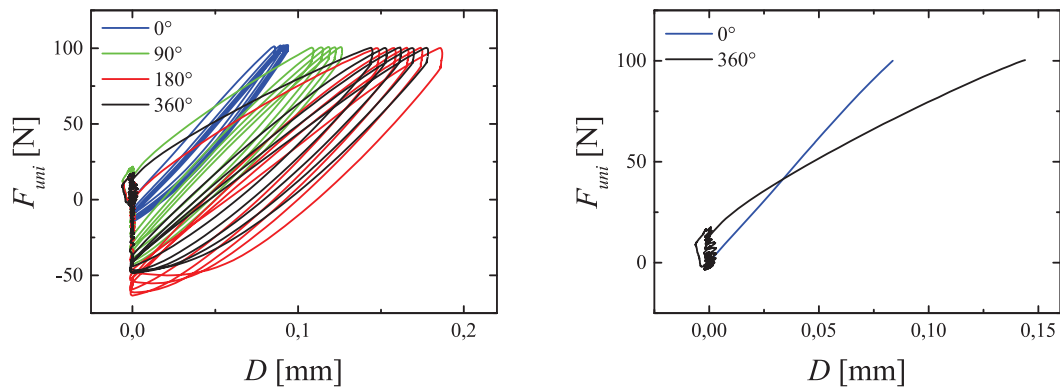


Figure 11: Left: Influence of pretorsion on the behavior in cyclic tensile test. Right: Loading paths of the first cycles for 0° and 360° pretorsion.

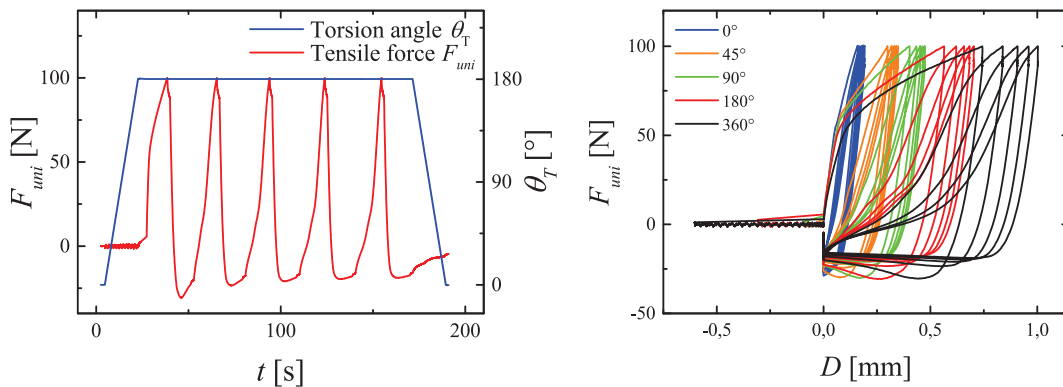


Figure 12: Left: Adapted experimental procedure in order to achieve pure torsion. Right: Influence of pure pretorsion on behavior in cyclic tensile test.

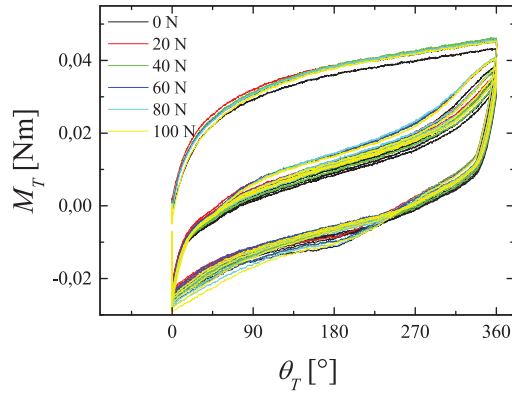


Figure 13: Influence of prestretch on cyclic torsion behavior.

3.2 Simulation

Similar to van der Heijden et al. [5, 6], simulations of these experiments based on our implementation of a Cosserat rod have been performed for the material parameters of nitinol. The results are shown in figure 6 in comparison to the theoretical curves of van der Heijden. These results, obtained based on an elastic constitutive law, show good agreement to the theoretical results. Since the experimentally measured curves deviate not only *quantitatively*, but also *qualitatively* from this theoretical shape, it is necessary to include viscoplastic effects in the modeling of the multiaxial deformation of cables.

4 CONCLUSIONS & OUTLOOK

The results of the classical and multiaxial experiments show the necessity of including viscoplastic effects in the description of cables. Since these effects have to be measured and observed in experiments at first, suitable experimental procedures enabling access to the material parameters have to be developed. Three kinds of multiaxial experiments have been executed in this work. In the case of viscoplastic cables, the interpretation of the writhing experiment is too complicated and will thus be used as a verification experiment. However, the combination of cyclic tension and torsion is a first step towards the design of interpretable multiaxial experiments for the characterization of viscoplastic cables. Similar experiments combining torsion and bending will be designed in future work, because the primary interest lies in viscoplasticity herein. Furthermore, suitable constitutive laws in accordance to the observed hysteresis curves have to be designed. They will be adapted in analogy to three-dimensional constitutive laws but formulated in the terms of sectional kinetic quantities of Cosserat rods.

REFERENCES

- [1] J. C. Simo. A finite strain beam formulation: the three dimensional dynamic problem - Part I. *Computer Methods in Applied Mechanics and Engineering*, Vol. 49, No. 1, pp. 55–70, 1985.
- [2] H. Lang, J. Linn, A. Tuganov. Geometrically exact Cosserat rods with Kelvin–Voigt type viscous damping. *Mechanical Sciences*, Vol. 4, pp. 79–96, 2013.
- [3] O. A. Bauchau, Z. Lao, M. Lyu, S. Brändle, J. Linn. Formulation of viscoelastic constitutive laws for beams in flexible multibody dynamics. *Proceedings of the IMSD, Busan, Korea*, 2014.
- [4] J. C. Simo, K. D. Hjelmstad, R. L. Taylor. Numerical formulations for finite deformation problems of beams accounting for the effect of transverse shear. *Computer Methods in Applied Mechanics and Engineering*, Vol. 42, pp. 301–330, 1984.
- [5] G. H. M. van der Heijden, S. Neukirch, V. G. A. Goss, J. M. T. Thompson. Instability and self-contact phenomena in the writhing of clamped rods. *International Journal of Mechanical Sciences*, Vol. 45, No. 1, pp. 161–196, 2003.
- [6] V. G. A. Goss, G. H. M. van der Heijden, J. M. T. Thompson, S. Neukirch. Experiments on Snap Buckling, Hysteresis and Loop Formation in Twisted Rods. *Experimental Mechanics*, Vol. 45, No. 2, pp. 101–111, 2005.
- [7] S. S. Antman. *Nonlinear Problems of Elasticity*. Springer, 2005.
- [8] E. H. Dill. Kirchhoff’s Theory of Rods. *Archives for history of exact sciences*, Vol. 44, No. 1, pp. 1–23, 1992.
- [9] J. C. Simo, T. J. R. Hughes. *Computational Inelasticity*. Springer, New York, 1998.
- [10] F. Armero. Elastoplastic and Viscoplastic Deformations in Solids and Structures. In E. Stein, R. de Borst, T.J.R. Hughes (Ed.). *Encyclopedia of Computational Mechanics*, Vol. 2, Ch. 7, John Wiley & Sons, 2004.
- [11] R. S. Rivlin, D. W. Saunders. Large elastic deformations of isotropic materials. VII. Experiments on the deformation of rubber. *Philosophical transactions of the Royal Society of London A*, Vol. 243, pp. 251–288, 1951.
- [12] H. Baaser, R. Noll. Simulation von Elastomerbauteilen - Materialmodelle und Versuche zur Parameterbestimmung. *DVM-Tag*, 2009.
- [13] M. Johlitz, S. Diebels. Characterisation of a polymer using biaxial tension tests. Part I: Hyperelasticity. *Archive of Applied Mechanics*, Vol. 81, pp. 1333–1349, 2011.
- [14] Z. Chen, T. Scheffer, H. Seibert, S. Diebels. Macroindentation of a soft polymer: Identification of hyperelasticity and validation by uni/biaxial tensile tests. *Mechanics of Materials*, Vol. 64, pp. 111–127, 2013.
- [15] S. P. Timoshenko, J. M. Gere. *Mechanics of Materials*. Van Nostrand Reinhold Company, New York, 1972.
- [16] L. Euler. Additamentum I de curvis elasticis, methodus inveniendi lineas curvas maximi minimi proprietate gaudentes. Lausanne, 1744, reprinted in *Opera Omnia I*, Vol. 24, pp. 231–297, 1960.
- [17] S. P. Timoshenko, J. M. Gere. *Theory of Elastic Stability*. McGraw-Hill Book Company, New York, 1961.